ELSEVIER

Colloids and Surfaces
A: Physicochemical and Engineering Aspects 142 (1998) 201–218

COLLOIDS AND SURFACES A

Growth of rod-like micelles in anionic surfactant solutions in the presence of Ca^{2+} counterions

R.G. Alargova [a], V.P. Ivanova [a], P.A. Kralchevsky [a,*], A. Mehreteab [b], G. Broze [c]

[a] *Laboratory of Thermodynamics and Physico-chemical Hydrodynamics, Faculty of Chemistry, University of Sofia, 1126 Sofia, Bulgaria*

[b] *Colgate-Palmolive Co., Technology Center, 909 River Road, Piscataway, NJ 08854-5596, USA*

[c] *Colgate–Palmolive Research and Development Inc., Avenue Du Parc Industriel, B-4041 Milmort, (Herstal), Belgium*

Received 7 November 1997; accepted 21 January 1998

Abstract

The experimental data for the growth of rod-like surfactant micelles in the presence of a 2:1 electrolyte ($CaCl_2$) do not comply with the available theory, which was originally developed for a 1:1 electrolyte. To solve the problem we undertook experimental and theoretical investigations with micellar solutions of the anionic surfactant sodium dodecyl polyoxyethylene-2 sulfate. Independent dynamic and static light scattering measurements of micelle size demonstrate that the effect of micelle–micelle interactions is negligible for the solutions investigated. Ultrafiltration experiments reveal that a considerable part of the Ca^{2+} ions are associated with micelles. Since our experiments are carried out at a fixed surfactant-to-Ca^{2+} ratio, the parameter of micelle growth (the equilibrium constant of micellization) indirectly depends on the surfactant concentration through the electrolyte concentration. That dependence is derived theoretically. The model of micelle growth, extended in this way, compares well with the experimental data. The model provides a quantitative description of the micelle size and charge as functions of the surfactant and electrolyte concentrations. The rod-like micelles have lower surface charge density than the spherical micelles; this makes their growth energetically favorable.

Keywords: Cod-like micelles; Micellar growth; Light scattering; Bivalent counterions

1. Introduction

The formation of aggregates in aqueous solutions of surfactants is strongly influenced by the experimental conditions. The shape and the aggregation number of the formed micelles depend on the surfactant concentration [1], length of the surfactant hydrophobic chain [2–4], temperature and presence of electrolyte [5–14] which is especially pronounced in the case of ionic surfactants. The transition from small spherical to large cylindrical micelles in the presence of *monovalent* electrolyte has been investigated in details both experimentally and theoretically [4–6,12]. It was recently established [15] that the presence of *multivalent* counterions (Ca^{2+}, Al^{3+}) in solutions of anionic surfactant (sodium dodecyl dioxyethylene sulfate: SDP2S) strongly enhances the formation of rod-like micelles. This observation can be qualitatively explained by the fact that one multivalent counterion, Ca^{2+} or Al^{3+}, can bind together two or more anionic surfactant headgroups at the micelle surface, thus decreasing the

* Corresponding author. Fax: 00359 681030;
e-mail: peter.kralchevsky@ltph.bol.bg

0927-7757/98/$ – see front matter
PII S0927-7757(98)00266-0

optimal area per headgroup [15]. This induces a transition from spherical to cylindrical micelles in accordance with the theory by Israelachvili et al. [1,16]. It was found [15,17] that at the same surfactant concentration the sphere-to-rod transition with Al^{3+} takes place at much lower ionic strength compared with the case with Na^{+}. In addition, it was established that the transition happens close to the value $\xi=1$ with ξ being the surfactant to aluminum ratio, $\xi \equiv c_{SM}/(Zc_{AT})$ (c_{SM} is the concentration of surfactant incorporated in the micelles, $Z=3$ is the counterion valence, c_{AT} is the Al^{3+} total concentration). In fact, $\xi=1$ corresponds to one Al^{3+} ion per three surfactant headgroups.

The situation with the bivalent Ca^{2+} ions is somewhat different. The experiment [15] shows that in this case the SDP2S micelles undergo a sphere-to-rod transition at smaller values of ξ — between 0.2 and 0.3 (instead of $\xi=1$ for Al^{3+}). This means that the total concentration of Ca^{2+} counterions needed for the transition to occur is from 3 to 5 times greater than the amount, which is necessary for the neutralization of the micellar surface ionizable groups. Similar is the situation with other bivalent counterions — see Fig. 1 in Ref. [15]. In the presence of bivalent counterions the sphere-to-rod transition occurs at ionic strength, which is larger than that in the case with Al^{3+}, but is still much smaller than that in the presence of Na^{+} counterions.

An additional motivation of our present study is the experimental fact that the large cylindrical micelles formed in the presence of Ca^{2+} and Al^{3+} exhibit a markedly larger solubilization efficiency than the common spherical micelles (see Fig. 10 in Ref. [15]). That is, the same amount of surfactant solubilizes more oil when it is organized as large cylindrical (rather than small spherical) micelles. This finding could be employed in detergency.

It was established [15,17] that the process of micelle growth, in the presence of Ca^{2+} or Al^{3+}, can not be interpreted by a direct application of the available theories [4–6,12] developed for the case of *monovalent* electrolyte. To solve the problem we accumulated additional experimental data which were further theoretically analyzed. The results, which are reported below in this paper, show that the data can be theoretically interpreted on the basis of an appropriate extension of the model by Missel et al. [6] (the "ladder model"). This model was recently applied to mixed micelles [18] and modified to account for temperature effects with nonionics [19]. The model has been confirmed by several experimental works [4,11–13].

It is known from the experiment, that the micelles of aggregation number greater than a certain value, n_0, are stable, whereas the aggregates of smaller aggregation number, $1<n<n_0$, are unstable. Missel et al. [6] have supposed that the micelles of aggregation number $n=n_0$ are spherical, and that the bigger micelles have a sphero-cylindrical shape (see Fig. 1). In other words, each micelle consists of a cylindrical part containing $n-n_0$ molecules and two hemispherical end-caps each of them containing $n_0/2$ molecules (Fig. 1). The theory of Missel et al. [6], as well as the earlier theory by Mukerjee [20], predicts, that the mass averaged aggregation number,

$$\bar{n}_M \equiv \frac{\sum_{n=n_0}^{\infty} n^2 X_n}{\sum_{n=n_0}^{\infty} nX_n}, \quad (1)$$

must increase proportionally to the square root of surfactant concentration:

$$\bar{n}_M \approx n_0 + 2[K(X-X_1)]^{1/2}, \quad (2)$$

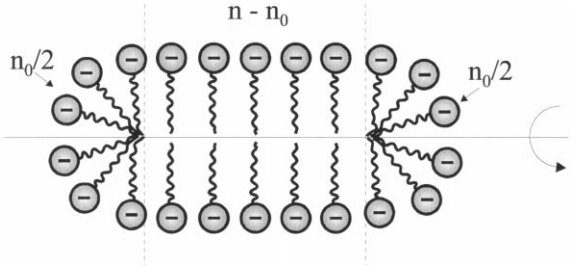

Fig. 1. Sketch of a rod-like micelle containing n surfactant molecules; n_0 is the number of molecules belonging to the hemispherical caps of the micelle. The hydrophilic headgroup of SDP2S contains two ethylene-oxide groups and one SO_4^- group.

where

$$X \equiv X_1 + \sum_{n \geq n_0} nX_n,$$

is the total molar fraction of the surfactant in the solution ($X = X_1$ at CMC), X_1 and X_n are the mole fractions of monomers and micelles of aggregation number n in the solution;

$$K \equiv \exp[(\mu^0_{n_0} - n_0\mu^0)/k_B T], \quad (3)$$

has the meaning of equilibrium constant of micellization or a parameter of micelle growth; here $\mu^0_{n_0}$ is the standard chemical potential of a (spherical) micelle of aggregation number n_0 and μ^0 is the standard chemical potential of a monomer in a cylindrical micelle, k_B is the Boltzmann constant, T is temperature. It should be noted that the ladder model accounts for their size distribution.

Our experimental data for SDP2S in the presence of $CaCl_2 + NaCl$ do not comply with Eq. (2) (for details see Section 2.3 below). The latter fact can be attributed to the effect of the added electrolyte on the electrostatic interactions in the system. One can distinguish two types of electrostatic effects in micellar solutions of ionic surfactants:

(1) Electrostatic *energy of micellization*: this is the work to bring a charged surfactant monomer from "infinity" across the electric double layer and to incorporate this monomer within a micelle, see Refs [12,21,22].
(2) Electrostatic interaction *between the micelles* in solution: this effect can be important for higher micelle concentrations and/or lower electrolyte concentrations; it is investigated in Refs [7,23–25].

Our analysis (see below) shows that for the studied system effect (2) is negligible, whereas effect (1) is of primary importance. In the next section we present and discuss experimental data obtained by laser light scattering and ultrafiltration. Next, we propose a quantitative interpretation of the experimental findings. We pay a special attention to the dependence of the growth parameter K on the electrolyte concentration and to the binding of Ca^{2+} ions to the micelles. The results reveal the cause of the micelle growth and give information about the surface charge of the micelles and its variation with the length of the rod-like aggregates.

2. Experimental results and preliminary discussion

2.1. Materials and solutions

The surfactant used in the present work is sodium dodecyl-dioxyethylene sulfate (SDP2S) with structure $CH_3(CH_2)_{11}(OC_2H_4)_2OSO_3Na$ (Empicol ESB70, Wilson Co., UK). The ionic strength resulting from the added electrolyte was $I_0 = 0.128$ M in all experiments. I_0 was adjusted constant by mixing NaCl and $CaCl_2 \cdot 2H_2O$ (Sigma) at various compositions. All micellar solutions were prepared using deionized water (Milli-Q, Organex grade). The surfactant concentration was varied between 3 and 8 mM (it is below 1 vol.%, i.e. low enough to avoid multiple light scattering from the micelles).

We studied the micelle growth with the increase of the surfactant concentration at fixed value of the surfactant-to-calcium ratio, ξ, which is defined as follows:

$$\xi = c_{SM}/(Zc_{CT}). \quad (4)$$

Here c_{CT} is the total concentration of the multivalent counterions (in our case Ca^{2+}) in the solution, and Z is their valence ($Z = 2$ for calcium).

We assume that the critical micellization concentration (CMC) does not depend on the ratio of Ca^{2+} to Na^+ at constant total ionic strength. This assumption is justified since CMC depends mostly on the total ionic strength, I_0, and rather weakly on the specific type of the dissolved micro-ions [26,27], which was confirmed also by our previous experiments [28]. The latter experiments with SDP2S showed that ln (CMC) decreases linearly with $\ln I_0$ in the concentration range $0.024 < 0.128$ M:

$$\ln \mathrm{CMC} = -11.444 - 0.7573 \ln I_0. \quad (5)$$

Similar dependence has been established experimentally for other surfactants [29]. The temperature was maintained 27 ± 0.1°C in all experiments.

2.2. Dynamic and static light scattering experiments.

The light scattering experiments were performed by means of Malvern 4700C System, supplied with Argon laser, operating at wavelength 488 nm, and K7032CE 8-Multibit 128-channel correlator. Before the measurements all solutions were filtered with Millipore 100 and 220 nm filters in order to remove dust particles.

We determined the mass-average diffusion coefficient of the micelles, D, using dynamic light scattering (DLS) and the micelle radius of gyration, R_G, using static light scattering, (SLS). Geometrical parameters of micelle shape are determined from the diffusion coefficient data [15]. For micelles of *spherical* shape one can calculate the micellar hydrodynamic radius, R_H, by means of the known Stokes–Einstein formula, $D=kT/(6\pi\eta R_H)$ The light scattering method gives the following evidences for the growth of rod-like micelles.

(1) The hydrodynamic radius, R_H, increases with the raise of the surfactant mole fraction, X, in the same way as it is in Fig. 1 of Ref. [6] or in Fig. 3 of Ref. [15].
(2) The plot of D versus X deviates from a straight line. As pointed out by Mazer [7], this deviation should be interpreted as a growth of larger micelles, rather than as a micelle–micelle attraction. (Indeed, if one attributes the deviation to van der Waals inter-micellar attraction, one will calculate unrealistically large values of the Hamaker constant.)
(3) The experimentally determined ratio R_G/R_H , with R_G being the radius of gyration, is systematically ≥ 2, which is typical for rigid rods, see Fig. 7 in Ref. [15] and the discussion therein.

In the case of *rod-like* micelles (Fig. 1) from the experimental time dependence of the autocorrelation function one can calculate the mass-average length of the rod-like micelles, L, using the same model as in Ref. 15; L equals the length of the cylinder plus the radii of the two hemispherical caps (Fig. 1), see the next subsection for more details. In particular, we assume that the radius of the rod is constant and equal to the extended length of one surfactant molecule, whereas the micelle length L can vary with the surfactant and electrolyte concentrations. The micelle length determined in this way (from the apparent hydrodynamic radius of the micelle, R_H) we denote by L_H.

On the other hand, L can be independently determined by static light scattering, from the *angular* dependence of the scattered light intensity using Eqs. (2.15), (2.16) and (3.3) in Ref. [15]. The value of L determined in this way (from the radius of gyration of the rods, R_G) we denote by L_G.

In Fig. 2 we plot L_H versus L_G for solutions of SDP2S in the presence of NaCl and $CaCl_2$. All experiments are performed at ionic strength $I_0=128$ mM. The empty circles are measured at $\xi=0.093$, the solid circles — at $\xi=0.110$, and the solid boxes — at $\xi=0.150$. Various experimental points denoted with the same symbol (Fig. 2) correspond to the same ξ, but to various surfactant concentrations. The dashed line in this figure corresponds to $L_H=L_G$. The experimental points are well described by this line in the framework of the experimental error, which can be up to 10%–15% for the smallest micelles and 5%–7% for the largest ones. This means that the micelle–micelle interactions do not affect significantly the micelle sizes measured by DLS. Indeed, to calculate L_H we use

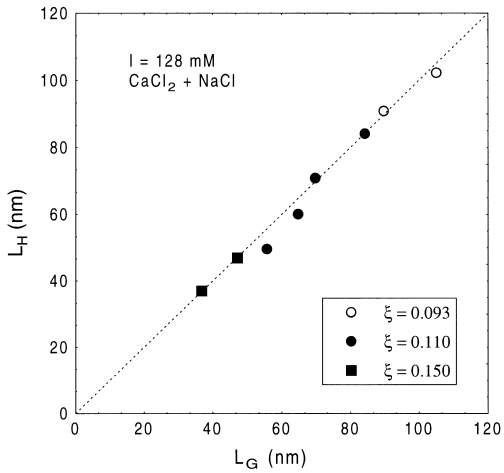

Fig. 2. Plot of L_H versus L_G for various ξ at fixed ionic strength $I_0=128$ mM. L_H and L_G denote length of a micelle calculated from the micelle hydrodynamic and gyration radius, respectively. The straight line corresponds to $L_H=L_G$.

expressions for the diffusion coefficient which are strictly valid for non-interacting micelles (hard rods). On the other hand, L_G is practically independent on the interactions between the micelles (see Ref. [15] for details). For that reason one can conclude that a pronounced effect of the interactions on dynamic light scattering data does not exist in the investigated range of salt and surfactant concentrations. Indeed, the influence of the interactions on L_H, should result in differences between the values of L_H and L_G varying with ξ, which is not observed (Fig. 2). This is not surprising because we deal with rather diluted micellar solutions (the average distance between the micelles is typically greater than their average length). The latter conclusion is confirmed by the criterion proposed by Missel et al. [12]. Comparing theory and experiment these authors established that the micelle–micelle interactions become important only when [12]

$$\frac{X}{X^*} = \frac{R_g}{2}\left(\frac{4\pi}{3V_m}\right)^{1/3} \geq 0.45. \quad (6)$$

Here R_g is the average micelle radius of gyration, $V_m = 18n_M/[(X-X_1)N_A]$, with N_A being the Avogadro number, is the average volume per micelle in the solution, X^* is the surfactant molar fraction at which the mean distance between the micelles is equal to the mean micellar radius of gyration. For the solutions investigated by us $X/X^* \leq 0.22$, and according to Eq. (6) the micelle–micelle interactions must be negligible. To make this estimate we used the experimentally measured values of R_g, For example, with the largest surfactant concentration. $c_s = 8$ mM, and $\xi = 0.093$ we measured $R_g = 22$ nm; for comparison, the Debye screening length (see Eq. (26) below) is much smaller, $\kappa^{-1} \approx 0.85$ nm.

2.3. Mass average aggregation number

Following the procedure described in Ref. [15] we calculated the micelle aggregation number, $\bar{n}_M$, using the radius and the length of the spherocylinders determined from the dynamic light scattering data (see Section 2.2). The procedure itself is the following.

(1) From the measured autocorrelation function of the scattered intensity one calculates the mass-average diffusion coefficient, D, using Eq. (2.6) in Ref. [15]. (2) For the smallest *spherical* micelles from the value of D one calculates the outer (hydrodynamic) radius of the micelle, $R_{out} = R_H$; the value of R_{out} thus obtained coincides (in the framework of the experimental accuracy) with the value $R_{out} = 2.77$ nm determined from literature data [1,26] for the lengths of the constitutive fragments of a SDP2S molecule. The radius of the cross-section of a rod-like micelle is assumed to be equal to R_{out}. (3) From the value of D for the *rod-like* micelles one calculates their average length, L, by using Eqs. (2.8)–(2.14) in Ref. [15]; L includes the length of the cylinder and the two hemispherical caps, see Fig. 1. (4) The average volume of the hydrophobic core of a micelle, V_{core} is then calculated from the values of L and R_{out} by using the following geometrical relationship:

$$V_{core} = \pi(R_{out} - l_{head})^2(L - 2R_{out}) + \frac{4}{3}\pi(R_{out} - l_{head})^3. \quad (7)$$

Here $l_{head} = 1.1$ nm is the length of the hydrophilic headgroup of a SDP2S molecule (two oxyethylene groups + one SO_4^- group) determined from literature data [1,26]. (5) Finally, we calculate the average aggregation number,

$$\bar{n}_M = V_{core}/V_{tail}, \quad (8)$$

where V_{tail} is the volume occupied by the hydrocarbon tail of a single surfactant molecule; for a dodecyl chain the literature data [1,26] yield $V_{tail} = 0.3502$ nm^3.

First of all we verify whether the growth of SDP2S micelles in the presence of *monovalent* (1:1) electrolyte obeys Eq. (2). Indeed, the validity of Eq. (2) has been verified for other surfactants [6,12,13,30], but not with SDP2S. We carried out DLS measurements to determine the micelle mean mass aggregation number, $\bar{n}_M$, at variable SDP2S concentrations and fixed concentration of NaCl, $I_0 = 0.7$ M, without adding any other electrolyte. Fig. 3 presents the obtained values of $\bar{n}_M$ plotted versus $(X\text{-}X_1)^{1/2}$ in accordance with Eq. (2), i.e. in accordance with the model developed by Mukerjee

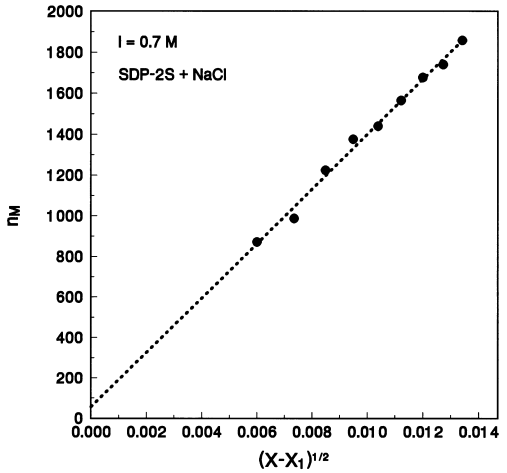

Fig. 3. Micelle mean mass aggregation number, $\bar{n}_M$, plotted versus $(X-X_1)^{1/2}$ in accordance with Eq. (2). All solutions contain 0.7 M NaCl, without any multivalent counterions.

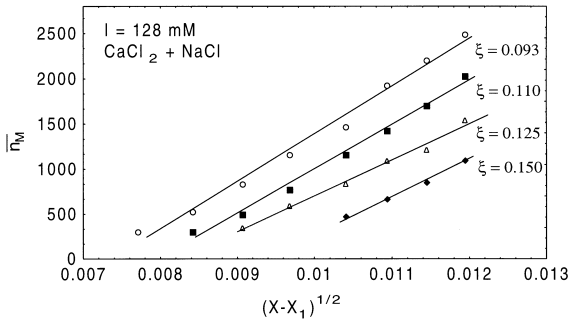

Fig. 4. Micellar mass average aggregation number $\bar{n}_M$ versus $(X-X_1)^{1/2}$ determined by dynamic light scattering from solutions of SDP2S at ionic strength $I_0=0.128$ M due to a mixture of Ca^{2+} and Na^+. For each curve ξ is kept constant, see Eq. (4).

[20] and Missel et al. [6]. One sees that the experimental data in Fig. 3 agrees well with a straight line, whose intercept is $n_0=57\pm6$. The latter value of the spherical micelle aggregation number is very reasonable. Indeed, the value of n_0, estimated from geometrical packing considerations [1] and experimental data for surfactant with the same hydrophobic tail, is about 60 monomers. Therefore, we conclude that in the presence of NaCl the growth of SDP2S micelles obeys Eq. (2).

Next, we determined $\bar{n}_M$ for solutions of the same surfactant, but with added electrolyte which is a mixture of $CaCl_2$ and NaCl at fixed ionic strength $I_0=0.128$ M. The surfactant mole fraction, X, and the surfactant-to-calcium ratio, ξ (see Eq. (4), were varied. Fig. 4 presents the obtained values of $\bar{n}_M$ plotted versus $(X-X_1)^{1/2}$ in accordance with Eq. (2). For each line ξ is kept constant. The dependencies should be straight lines with intercepts equal to the aggregation number of the smallest spherical micelles, $n_0\approx60$. One sees that the curves in Fig. 4 look like straight lines, but their intercepts are negative and, hence, physically meaningless. Therefore, one can conclude that the direct application of the "ladder" model, related to Eq. (2), cannot provide quantitative interpretation of the data for the micelle growth in solutions containing Ca^{2+} ions. One possible way to solve the problem is to take into account the dependence of the growth parameter, K (see Eq. (3), on the concentration of the ionic species, and especially, of the Ca^{2+} ions. To clarify this point we undertook ultrafiltration experiments described below.

2.4. Ultrafiltration experiments

The multivalent metal ions bind strongly to the negatively charged surface of the anionic micelles and therefore they can be partially removed from the solution by performing ultrafiltration experiment using a membrane with appropriate pore size [31,32]. Since all ions belonging to the Stern and diffuse parts of the electric double layers around the micelles are retained, the ultrafiltration experiment, performed with an appropriate membrane can be used to determine the background concentration of the multivalent ions in the micellar solution. It is reasonable to assume that the composition of the solution permeating through the pores of the ultrafiltration membrane is identical to that of the medium surrounding the micelles. We determined the background concentration of Ca^{2+}, c_{CB}, in 2, 4 and 8 mM SDP2S solutions at $I_0=128$ mM and at various values of the total input concentration of Ca^{2+}. The value of the surfactant-to-calcium ratio, ξ, was varied by varying the total input concentration of calcium, c_{CT}. The ultrafiltration experiments were carried out at room temperature ($22\pm2^\circ$C) in dead-end mode in

a 100 ml stirred cell at 0.5 atm transmembrane pressure. We used a polysulfonic membrane with molecular weight cut-off 6000 Da which is low enough to permit the retention even of the smallest SDP2S micelles. The concentration of Ca^{2+} in the permeate was determined spectro-photometrically [33], using the color reaction between murexide (ammonium purpurate, Sigma) and Ca^{2+}.

The experimental data for c_{CB}/c_{SM} and c_{CB}/c_{CT} versus ξ for $c_s=8$ mM are plotted in Fig. 5(a); $c_{SM}=c_s-CMC$ is the concentration of the surfactant built in the micelles and c_s is the total surfactant concentration. One can see that the ratio c_{CB}/c_{CT} varies between 0.75 and 0.40, which means that for $0.1<\xi<0.8$ from 25% up to 60% of the Ca^{2+} ions are bonded to the micelles. In this aspect there is a great difference with the micelle growth in solutions of 1:1 electrolyte, in which the amount of counterions associated with the micelles is negligible in sense that it does not affect the bulk concentration of the ionic species [6,12].

To interpret the data in Fig. 4 we need to know what is the calcium background concentration, c_{CB}, corresponding to a given total calcium concentration c_{CT} at various surfactant concentrations, c_s. To obtain this dependence we use model considerations based on the mass balance of Ca^{2+} in the solution, which is given by the expression

$$c_{CT}=c_{CB}+\Gamma_c a_H c_{SM} \quad (c_{SM}\equiv c_s-CMC), \tag{9}$$

where a_H is the area per surfactant headgroup in the micelles and Γ_c denotes the number of associated Ca^{2+} ions per unit area of the micelle surface. (Here, for the sake of simplicity all Ca^{2+} counterions belonging to the Stern and diffuse layers are treated in the same way.) To estimate Γ_c we use the Langmuir adsorption isotherm

$$\Gamma_c=\Gamma_\infty\frac{c_{CB}}{B+c_{CB}};\quad \Gamma_\infty\approx(2a_H)^{-1}. \tag{10}$$

Here B is a constant related to the energy of Ca^{2+} adsorption and Γ_∞ is the maximum possible adsorption corresponding to the case when each couple of surfactant headgroups is electro-neutralized by one Ca^{2+} ion. Next, in Eq. (9) we substitute Γ_c from Eq. (10) and $c_{CT}=c_{SM}/2\xi$ to derive

$$2\xi x^2+(\xi+2E\xi-1)x-E=0, \tag{11}$$

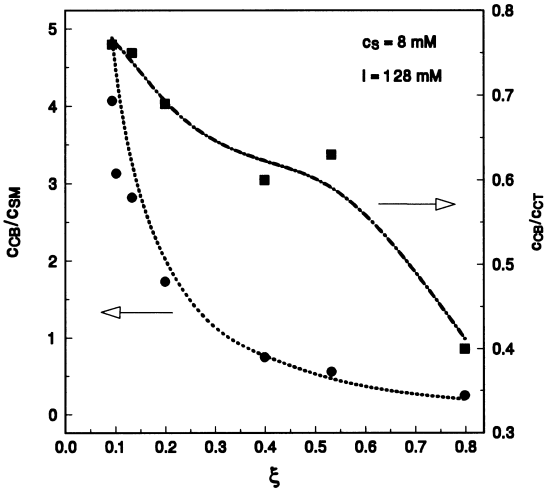

(a)

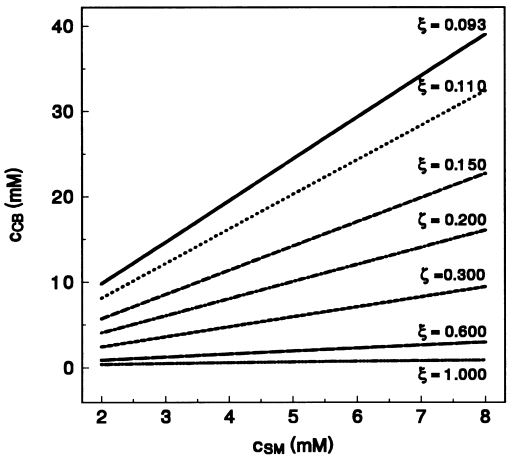

(b)

Fig. 5. (a) Plots of ultrafiltration data for c_{CB}/c_{SM} and c_{CB}/c_{CT} versus ξ for fixed $c_s=8$ mM and $I=128$ mM. The dotted line is drawn by means of Eqs. (12) and (13) for $B=0.025$ mM. (b) Theoretical dependencies of c_{CB} on c_{SM} calculated from the same equations with $B=0.25$ mM and various ξ.

where we have introduced the notation

$$x=\frac{c_{CB}}{c_{SM}},\ E=\frac{B}{c_{SM}}. \tag{12}$$

Solving Eq. (11) we obtain

$$x=\frac{1}{4\xi}\{-(\xi+2E\xi-1)+[(\xi+2E\xi-1)^2+8E\xi]^{1/2}\} \tag{13}$$

We have selected the physical root of Eq. (11) which gives $x \to 0$ (no Ca^{2+} in the permeate) for $\xi \to \infty$ (no Ca^{2+} in solution).

We fitted the experimental data for $c_s = 2$, 4 and 8 mM with Eq. (13) and determined the value of the adsorption constant $B = 2.5 \times 10^{-5}$ M. The dotted line in Fig. 5(a) is drawn by means of Eq. (13) with the latter value of B. The agreement between theory and experiment seems quite satisfactory in view of the low accuracy of the determination of c_{CB} by the spectro-photometric method and the simplifications made when deriving Eq. (13).

Next we calculate the dependence of c_{CB} on c_{SM} using the Eqs. (12) and (13) with $B = 2.5 \times 10^{-5}$ M for the values of ξ corresponding to the experimental curves in Fig. 4. The results are shown in Fig. 5(b). It is seen that the background concentration of the unbound Ca^{2+}, c_{CB}, changes significantly with the surfactant concentration c_{SM}. This is due to the fact that a considerable part of the Ca^{2+} ions in the solutions are attached to the micelle surfactant headgroups. The increase of c_{CB} with c_{SM} is easy to understand having in mind that calcium and surfactant are added in the solution at a fixed proportion, ξ, see Eq. (4).

In general, the background Ca^{2+} concentration, c_{CB}, influences the energy of the micelle electric double layer. Therefore, the growth parameter becomes dependent on c_{CB}, that is $K = K(c_{CB})$. In addition, at fixed ξ the background calcium concentration is dependent on the surfactant concentration: $c_{CB} = c_{CB}(c_{SM})$, [see Fig. 5(b)], Thus it turns out that at fixed ξ the growth parameter is an indirect function of the surfactant concentration: $K = K[c_{CB}(c_{SM})]$. This dependence must be taken into account in order to interpret the data for $\bar{n}_M$ versus $(X\text{-}X_1)^{1/2}$ presented in Fig. 4 (note that $X - X_1 = 0.018 c_{SM}$ if c_{SM} is expressed in mol/l). The theory of the double layer contribution into K is presented in the Section 4 below.

3. The true ionic strength of solution

The binding of Ca^{2+} ions to the micelle surface is accompanied by release of Na^+ ions from the micelles. The background concentration of the Na^+ ions, c_{NB}, can be calculated by means of the following expression:

$$c_{NB} = c_{NT} + 2(c_{CT} - c_{CB}) + [c_{SM} - 2(c_{CT} - c_{CB})]\alpha_{Na} + \mathrm{CMC}. \quad (14)$$

Here c_{NT} expresses the total input concentration of Na^+ from the dissolved NaCl; the term $2(c_{CT} - c_{CB})$ stands for the Na^+ counterions replaced from the double layer around each micelle by the adsorbed Ca^{2+} ions; the next term, $[c_{SM} - 2(c_{CT} - c_{CB})]\alpha_{Na}$, accounts for the Na^+ ions dissociated from the micelle headgroups, which are not occupied by adsorbed Ca^{2+}; α_{Na} denotes the average degree of charging of the micelle headgroups, which are free of adsorbed Ca^{2+} ($0 < \alpha_{Na} < 1$); the fact that α_{Na}, is less than 1 accounts for adsorption of Na^+ in the micelle Stern layer; finally the term CMC in Eq. (14) stands for the Na^+ ions dissociated from the free surfactant monomers in the solution. As mentioned earlier, in our experiments the apparent ionic strength of the input electrolyte, I_0, is kept constant ($I_0 \equiv 128$ mM):

$$c_{NT} + 3c_{CT} = I_0 \equiv \mathrm{constant}. \quad (15)$$

Next, the true background ionic strength of the solution can be calculated:

$$I_t = \frac{1}{2}[4c_{CB} + c_{NB} + (2c_{CT} + c_{NT}) + \mathrm{CMC}]. \quad (16)$$

The term $2c_{CT} + c_{NT}$ in the parenthesis expresses the concentration of the Cl^- ions dissociated from the dissolved $CaCl_2$ and NaCl, and the last term (CMC) in Eq. (16) accounts for the present of ionized surfactant monomers in the solution. The substitution of c_{NB} and c_{NT} from Eqs. (14) and (15) into Eq. (16) yields

$$I_t = I_0 + c_{CB} - c_{CT} + \mathrm{CMC} + \frac{1}{2}(c_{SM} + 2c_{CT} - 2c_{CB})\alpha_{Na}. \quad (17)$$

In our calculations we take into account also the fact that the critical micellization concentration

(CMC) depends on the ionic strength, see Eq. (5):

$$c_{SM} = c_s - CMC(I_t); \quad c^0_{SM} = c_s - CMC(I_0);$$
$$c_{CT} \equiv \frac{c^0_{SM}}{2\xi}. \tag{18}$$

Let us mention in advance that for the solutions studied by us the true ionic strength, I_t, calculated from Eq. (17), appears to be close to $I_0 = 128$ mM and is not sensitive to the variation of ξ. Moreover, $CMC(I_0) \approx 0.05$ mM is very low compared to I_0, and therefore gives a negligible contribution to I_t.

4. Electrostatic contribution to the micelle growth parameter

4.1. Electrostatic interactions and growth parameter

The energy of the micelle double layer gives a contribution to the standard chemical potential of a surfactant molecule incorporated into a micelle, and consequently, to the growth parameter, K:

$$K = K_{dl} K_{ndl}, \tag{19}$$

where K_{dl} and K_{ndl} denote the *double layer* and *non-double layer* contribution into the growth parameter, see Eq. (3). K_{dl} can be expressed in the form [6,12]

$$\ln K_{dl} = \frac{n_0(g^{el}_s - g^{el}_c)}{kT}, \tag{20}$$

where g^{el} presents the electrostatic energy per surfactant molecule incorporated into a micelle; subscripts "s" and "c" denote "spherical" and "cylindrical" micelle, respectively. Theoretical expressions for g^{el} have been derived in Refs [21] and [12] for the case of a symmetrical (1:1) electrolyte, and in Ref. [17] for the mixture of 1:1 and 3:1 electrolytes (NaCl and $AlCl_3$). To interpret the results, measured in the presence of $CaCl_2$ and NaCl, we have to express theoretically g^{el} for surfactant solutions containing a mixture of 1:1 and 2:1 electrolytes. g^{el} can be calculated by means of the expression [21,34]

$$g^{el} = \frac{e}{|\sigma|} \int_0^{\sigma} \psi_0 \, d\sigma, \tag{21}$$

where e is the elementary charge, σ denotes the surface charge density and ψ_0 is the surface potential.

4.2. Expression for the surface charge density

To determine the dependence $\psi_0(\sigma)$ we have to solve the Poisson equation

$$\frac{d^2\psi}{dr^2} + \frac{m}{r}\frac{d\psi}{dr} = -\frac{4\pi}{\epsilon}\rho(r), \quad m = 0, 1, 2 \tag{22}$$

where ψ and ρ denote the electric potential and bulk charge density, r is the coordinate along the normal to the charged surface; $m = 0$ for flat surface, $m = 1$ for cylindrical and $m = 2$ for spherical surface; ρ can be expressed by means of the Boltzmann equation:

$$\rho = ec_{NB} \exp\left(-\frac{e\psi}{kT}\right) + 2ec_{CB} \times \exp\left(-\frac{2e\psi}{kT}\right) - e(c_{NB} + 2c_{CB}) \exp\left(\frac{e\psi}{kT}\right), \tag{23}$$

where c_{NB} and c_{CB} are the background concentrations of Na^+ and Ca^{2+}. Combining Eqs. (22) and (23) we obtain

$$\frac{d^2y}{dx^2} + \frac{m}{x}\frac{dy}{dx} = \sinh y + \lambda^2(e^{2y} - e^y - \sinh y), \tag{24}$$

where we have introduced the notation

$$x = \kappa r, \quad y = -\frac{e\psi}{kT}, \tag{25}$$

$$\kappa^2 = \frac{8\pi e^2 I_t}{\epsilon kT}, \quad \lambda^2 = \frac{c_{CB}}{I_t}. \tag{26}$$

In view of Eqs. (25) and (26) the boundary condition at the charged surface, $d\psi/dr = -4\pi\sigma/\epsilon$

can be presented in the form

$$\frac{dy}{dx}=\frac{4\pi\sigma e}{\epsilon kT\kappa}\equiv -S(y_0) \quad \text{(at the surface)}, \tag{27}$$

$$y_0\equiv y|_{x=\kappa R}. \tag{28}$$

In the case of cylindrical or spherical surface of radius R (corresponding to the surface at which the centers of the SO_4^- groups are located) the boundary condition is to be imposed at $x=\kappa R$. In general, $S\equiv -dy/dx$. Next we multiply Eq. (24) by dy/dx, integrate, and then set $y=0$ and $y'=0$ for $x\to\infty$; the result reads

$$\left(\frac{dy}{dx}\right)^2=4\sinh^2\left(\frac{y}{2}\right)[1-\lambda^2+\lambda^2e^y] + \int_x^\infty \frac{2m}{x}\left(\frac{dy}{dx}\right)^2 dx. \tag{29}$$

Following the procedure of Wiersmaa et al. [35], which has been also utilized by other authors [12,21,36], we use the approximation

$$\int_{\kappa R}^\infty \frac{1}{x}\left(\frac{dy}{dx}\right)^2 dx\approx -\frac{1}{\kappa R}\int_0^{y_0}\frac{dy}{dx}dy\equiv\frac{1}{\kappa R}J(y_0). \tag{30}$$

To estimate the last integral, denoted by J, we substitute dy/dx for a flat interface ($m=0$) [35], see Eq. (29):

$$\frac{dy}{dx}=-2\sinh\left(\frac{y}{2}\right)\sqrt{1-\lambda^2+\lambda^2e^y}. \tag{31}$$

Next, combining Eqs. (27)–(31) we derive

$$S(y)=\left\{4\sinh^2\left(\frac{y}{2}\right)[1-\lambda^2+\lambda^2e^y]+\frac{2m}{\kappa R}J(y)\right\}^{1/2}, \tag{32}$$

where

$$J(y)=\frac{1-3\lambda^2}{2\lambda}\ln\left[\frac{(\rho+\lambda)(1-\lambda)}{(\rho-\lambda)(1+\lambda)}\right] + (2+e^y)\rho-3; \quad \rho\equiv\sqrt{\lambda^2+(1-\lambda^2)e^{-y}}. \tag{33}$$

For $\lambda\to 0$ (no Ca^{2+} ions in the solution) one obtains $J\to 8\sinh^2(y/4)$ and Eq. (32) reduces to the expression of Mitchell and Ninham [21] for 1:1 electrolyte.

Finally, integrating by parts in Eq. (21) and making use of Eqs. (25)–(28) we derive

$$\frac{g^{el}}{kT}=\frac{e}{|\sigma|}\frac{kT}{e^2}\frac{\epsilon\kappa}{4\pi}\left[y_0S(y_0)-\int_0^{y_0}S(y)\,dy\right], \tag{34}$$

where $S(y)$ is to be substituted from Eq. (32), and $S(y_0)$ is determined by the boundary condition Eq. (27). The integration in Eq. (34) is to be carried out numerically. To obtain K_{dl} by means of Eq. (20) we calculate the values of g^{el} for spherical ($m=2$) and cylindrical ($m=1$) micelle, details about the procedure of calculations are given in the Appendix A.

4.3. Model of the Stern layer

The area per surfactant headgroup, a, calculated by us from the results for the micelle shape and aggregation $a_s=1.48\ nm^2$ for the *spherical* micelles and $a_c=0.64\ nm^2$ for the *cylindrical* ones (see the Appendix A for the calculation of a_s and a_c). These values are markedly larger than the area per molecule in a dense surfactant adsorption monolayer, which is ca. $0.35\ nm^2$. Therefore, it is possible some Ca^{2+} ions to be intercalculated among the surfactant headgroups at the micelle surface, thus partially neutralizing the surface charge of the micelles. In such a case

$$\sigma=-\alpha\frac{e}{a}, \tag{35}$$

where α is an *apparent* degree of dissociation (charging) of the ionizable headgroups on the surface of a micelle ($0<\alpha<1$). The parameter α expresses the fraction of the "nonneutralized" headgroups:

$$\alpha=1-\theta_C-\theta_N, \tag{36}$$

where θ_C and θ_N are the occupancies of the Stern layer by Ca^{2+} and Na^+ ions [37]:

$$\theta_N=\frac{b_Nc_{NB}}{1+b_Nc_{NB}+b_Cc_{CB}},\ \theta_C\equiv\frac{2\Gamma_C}{\Gamma_s} =\frac{b_Cc_{CB}}{1+b_Nc_{NB}+b_Cc_{CB}} \tag{37}$$

Γ_s and Γ_C denote adsorption of surfactant and Ca^{2+}; the multiplier 2 accounts for the fact, that one Ca^{2+} ion neutralizes two surfactant headgroups. In fact, Eq. (37) represents Langmuir isotherms for the competitive adsorption of Ca^{2+} and Na^+ in the Stern layer. The adsorption parameters in Eq. (37) are to be determined from the expressions [37,38]

$$b_N = a\delta_N \exp\left(\frac{\Phi_N + y_0}{kT}\right),\ b_C = a\delta_C \exp\left(\frac{\Phi_C + 2y0}{kT}\right). \quad (38)$$

Here a ($=a_s$ or a_c) is the area per surfactant headgroup; $\delta_N = 0.72$ nm and $\delta_C = 0.82$ nm are the diameters of the hydrated Na^+ and Ca^{2+} ions [1]; Φ_N and Φ_C are the specific adsorption energies of the respective ions. For high adsorption energy $\Phi_N \to \infty$ (or $\Phi_C \to \infty$) Eqs. (37) and (38) predict $\theta_N \to 1$ (or $\theta_C \to 1$), as could be expected.

To estimate Φ_N and Φ_C we use the following model. In general, Φ_C presents the work carried out to bring one Ca^{2+} ion from the subsurface to the surface. The points A, B and C in Fig. 6 denote the positions of three neighboring surfactant headgroups at the surface of a micelle; D denotes the position of a Ca^{2+} ion in the subsurface and P is the position of this ion when it is intercalated among the headgroups. Then we use the Coulomb low to estimate the work carried out to bring the Ca^{2+} ion from point D to point P; thus we obtain

$$\Phi_C = \frac{6e^2}{\epsilon_{st} kT}\left(\frac{1}{r_a} - \frac{1}{\sqrt{r_a^2 + \delta^2}}\right),\ r_a = \sqrt{\frac{2a}{3\sqrt{3}}}. \quad (39)$$

Here δ is the distance between points D and P (the thickness of the Stem layer) and r_a (see Fig. 6) is estimated assuming hexagonal packing of the surfactant headgroups; ϵ_{st} is the dielectric constant in the Stern layer, which is expected to be smaller than the dielectric constant of the bulk water because of the water molecules belonging to the hydration shells around the ions [29,39]. Likewise, one obtains an expression for Φ_N:

$$\Phi_N = \frac{3e^2}{\epsilon_{st} kT}\left(\frac{1}{r_a} - \frac{1}{\sqrt{r_a^2 + \delta^2}}\right). \quad (40)$$

Note that Eqs. (39) and (40) account for the interaction of the adsorbing counterion with the first-neighbor surface charges only. This is an appropriate approximation for the case, when the average surface charge density σ (and the degree of surface charging α) is relatively low. Indeed, in such a case the interaction of an adsorbing counterion with the second-neighbor *non-neutralized* surface charges can be neglected.

Now we have all equations necessary to calculate g^{el} and K_{dl}, see Eqs. (19) and (20). The procedure of calculations is described in Appendix A.

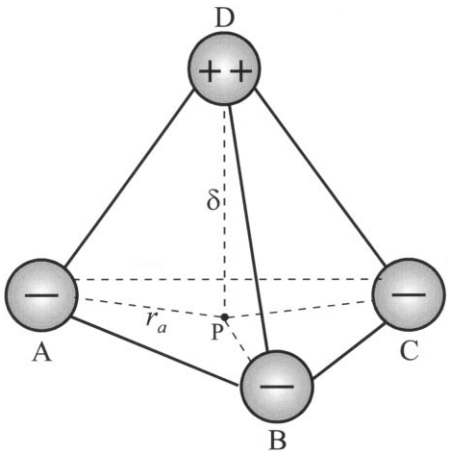

Fig. 6. To the derivation of Eq. (39); A, B, and C denote the positions of three surfactant headgroups; D and P denote the positions of a bivalent counterion in the subsurface and among the headgroups, respectively.

5. Numerical results and discussion

5.1. Processing of the experimental data

The aim of the numerical procedure is to fit the experimental data from Fig. 4 plotted as $\bar{n}_M$ versus $[K_{dl}(X - X_1)]^{1/2}$:

$$\bar{n}_M = n_0 + [2\sqrt{K_{ndl}}]q;\quad q \equiv [K_{dl}(X - X_1)]^{1/2} \quad (41)$$

Eq. (41) is corollary of Eqs. (1) and (19). $\bar{n}_M$ is given by the experiment as a function of the micelle concentration: $X - X_1 = 0.018\ (c_s - \mathrm{CMC}) = 0.018 c_{SM}$, where the values of c_s and CMC are

given in mol/l. The aggregation number of the smallest spherical micelles is also known from the experiment: $n_0 \approx 56$. The equations from the previous section allow the calculation of K_{dl} for a given value of X (see the Appendix A). As K_{ndl} is not expected to depend on X and ξ, Eq. (41) shows that the plot of $\bar{n}_M$ versus q should be a straight line. To fit the data we apply the least squares method; we minimize numerically the function

$$\Psi(\delta, K_{ndl}) = \sum_i [(\bar{n}_M)_i - \bar{n}_M(q_i)]^2, \quad (42)$$

where $(\bar{n}_M)_i$ and q_i are values of $\bar{n}_M$ and q calculated from the experimental data; $\bar{n}_M(q_i)$ is calculated substituting $q = q_i$ in Eq. (41); the summation in Eq. (42) is carried out over all experimental points. From the best fit of the data for $\xi = 0.093$ (see the respective curve in Fig. 4) we determine $\delta = 5.5$ Å and $K_{ndl} = 5.0 \times 10^8$. The data (the empty circles in Fig. 7) comply well with a straight line of intercept $n_0 = 56$.

Since K_{dl} is not expected to depend on ξ, we fixed $K_{ndl} = 5.0 \times 10^8$ and processed the data for the other values of ξ ($\xi = 0.110$, 0.125 and 0.150, cf. Fig. 4) with a single adjustable parameter, δ, see Eqs. (40) and (15). The values of δ determined from the best fits are listed in Table 1; all of them are between 5.48 and 5.52 Å, i.e. $\delta \approx 5.5$ Å, which is a physically reasonable result.

The largest micelles (the experimental points on the right in Fig. 7) have apparent hydrodynamic radius, R_H, about 20 nm (calculated from the measured diffusion coefficient by means of the Stokes–Einstein formula), whereas for the smallest investigated micelles (the experimental points on the left in Fig. 7) this value is $R_H \approx 3$ nm. The latter value is close to the limit of the Malvern light-scattering apparatus; moreover, the micelle concentration in this case is rather low. Therefore, the experimental error is the greatest for the smallest studied micelles.

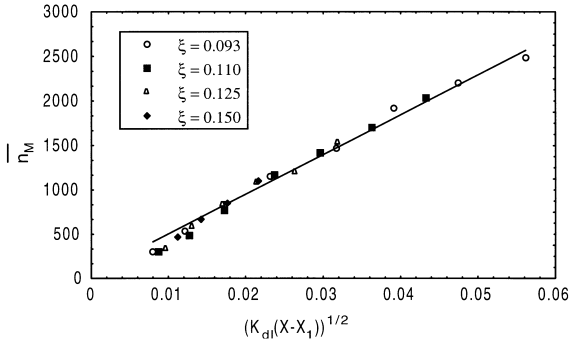

Fig. 7. The data for the micellar mass average aggregation number $\bar{n}_M$ from Fig. 4 plotted versus $[K_{dl}(X\text{-}X_1)]^{1/2}$ in accordance with Eq. (41).

Table 1
Parameter values determined from the fit in Fig. 7 for various surfactant-to-Ca^{2+} ratio ξ; the superscripts "c" and "s" denote cylindrical and spherical micelle, respectively

ξ	δ (Å)	Φ_C^c (kT)	Φ_C^s (kT)	Φ_N^c (kT)	Φ_N^s (kT)
0.093	5.51	3.96	1.51	1.98	0.76
0.110	5.52	3.97	1.52	1.98	0.76
0.125	5.49	3.94	1.50	1.97	0.75
0.150	5.48	3.93	1.50	1.97	0.75

One sees in Fig. 7 that data from all curves in Fig. 4, corresponding to $0.093 \leq \xi \leq 0.150$, can be fitted with the *same* straight line with intercept and slope corresponding to $n_0 = 56$ and $K_{ndl} = 5.0 \times 10^8$, see Eq. (41). This result means that the model of micelle growth by Missel et al. [6] is applicable to our experimental system if the effect of electrolyte on K_{dl} is accounted for as suggested in Section 4 above.

It should be noted, that all data are processed with the same value of the dielectric constant of the Stern layer: $\epsilon_{st} = 55.5$. This value provides the best fit of our data for Ca^{2+} ions and some new data for Al^{3+} ions [17]. The value $\epsilon_{st} = 55.5$ seems acceptable in so far as it is intermediate between $\epsilon = 78.3$ for the bulk water and $\epsilon \approx 32$ for the hydration shells of the ions [29,39].

5.2. Discussion

Having processed the experimental data for $\bar{n}_M$ versus $q \equiv (K_{dl}(X\text{-}X_1))^{1/2}$ (see Fig. 7) by means of the theoretical model from Section 4, we simultaneously obtain values of many physical parameters (such as adsorption energy, micelle surface charge and potential, electrostatic energy per monomer, etc.) which elucidate the physical picture and the cause of the micelle growth in the investigated system.

Let us start with the adsorption energies Φ_C and Φ_N calculated by means of Eqs. (39) and (40). Since the areas per headgroup for the cylindrical and spherical micelles are different ($a_c = 0.64$ nm^2; $a_s = 1.48$ nm^2, see the Appendix A) the respective values of Φ_C and Φ_N are different, see Table 1 and Eqs. (39) and (40); it turns out that the energy of counterion adsorption at cylindrical micelle is about 2.6 times larger than at spherical micelle; this fact can be attributed to the shorter distance between the surfactant headgroups at the surface of the cylindrical micelle. In addition, for micelles of the same shape, Φ_C is twice as large as Φ_N, owing to the double charge of Ca^{2+} as compared to Na^+. In summary, the data in Table 1 shows that δ is practically independent of ξ; one can work with $\delta \approx 5.5$ Å for all values of ξ.

Fig. 8 shows the background concentration of Na^+, c_{NB}, calculated by means of Eq. (14), see the Appendix A for details. The symbols in Fig. 8 denote the points at which measurements of the micelle aggregation number have been carried out, see Fig. 4 and 7. One sees that at the lower surfactant concentrations c_{NB} is close to 0.08 M, which is about 62% of the total ionic strength of the solution, $I_0 = 0.128$ M. With the increase of surfactant concentration at fixed ξ and ionic strength (see Eqs. (4) and (15) the Na^+ ions are replaced by Ca^{2+} ions and c_{NB} decreases. In spite of the lower adsorption energy of the Na^+ ions ($\Phi_N < \Phi_C$, see Table 1) they compete with Ca^{2+} ions for the adsorption in the Stern layer, especially at the lower values of $X - X_1$, at which c_{NB} is large compared with c_{CB}, cf. Fig. 5(b) and 8. The true ionic strength of the solutions, I_t, calculated from Eq. (17), appears to be close to $I_0 = 128$ mM and is not sensitive to the variation of ξ. It turns out that important is the variation of the surface charge of the micelles, see below.

In Ref. [12] it was established that the magnitude of the hydration radii of various alkali metal ions influences the micelle growth. In the present study this effect is accounted for through the parameters δ_N and δ_C in Eq. (38) above.

Fig. 9 presents the occupancy θ_C of the Stern layer by Ca^{2+} as a function of $q \equiv (K_{dl}(X - X_1))^{1/2}$ for the cases of cylindrical and spherical micelles and for various ξ. It is not surprising that θ_C is greater for the cylindrical micelles because they exhibit smaller distances between the surfactant headgroups, and consequently $\Phi_C^c > \Phi_C^s$, see Table 1. The increase of θ_C with the surfactant concentration can be attributed to the increase of the bulk Ca^{2+} concentration with the rise of $X - X_1$, see Fig. 5(b). At the larger surfactant concentrations θ_C approaches 87% for the cylindrical micelles (and 60% for the spherical ones), which means that the micelle surface charges are neutralized to a great extent, and that there is not much space left in the Stern layer for the adsorption of Na^+ ions, especially on the cylindrical micelles.

Fig. 10 shows the occupancy θ_N of the Stern layer by Na^+ ions. The latter may occupy adsorption sites free of Ca^{2+} and that is the reason why θ_N is larger for the spherical micelles, which bind

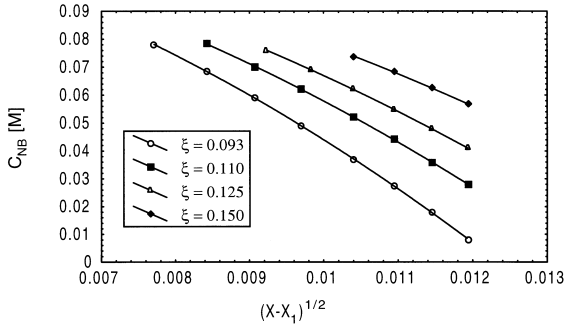

Fig. 8. Plot of the Na^+ background concentration c_{NB} versus $(X - X_1)^{1/2}$ for various values of the surfactant-to-Ca^{2+} ratio ξ.

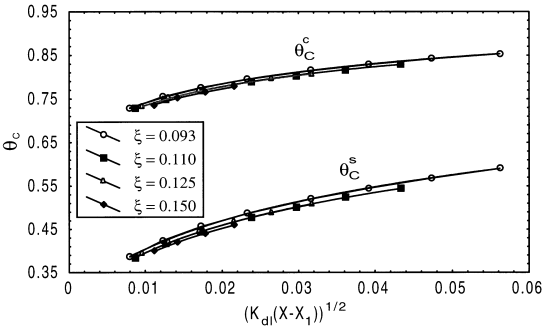

Fig. 9. Occupancy of the Stern layer by Ca^{2+} ions for cylindrical and spherical micelles: θ_C^c and θ_N^s, respectively, plotted versus $[K_{dl}(X\text{-}X_1)]^{1/2}$.

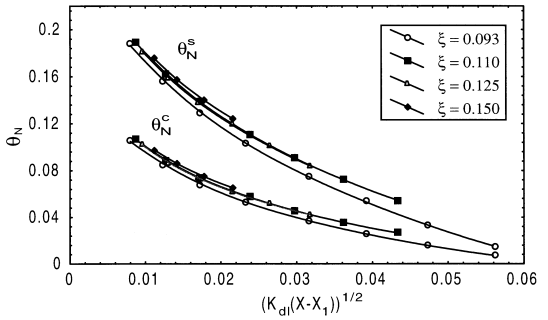

Fig. 10. Occupancy of the Stern layer by Na^+ ions for-cylindrical and spherical micelles: θ_C^c and θ_N^s, respectively, plotted versus $[K_{dl}(X\text{-}X_1)]^{1/2}$.

less Ca^{2+} than the cylindrical ones, cf. Fig. 9. Anyway, in these experiments θ_N may raise up to 19% (Fig. 10) and it should not be neglected when calculating the micelle surface charge.

Fig. 11 presents the calculated degree of charging α of the cylindrical and spherical micelles,see Eq. (36). One sees that α slightly decreases with the rise of $X-X_1$ which can be attributed to the fact that the background Ca^{2+} concentration, c_{CB}, and θ_C increase together with $X-X_1$, see Fig. 5(b) and Fig. 9. For the spherical micelles α varies between 39% and 43%, whereas for the cylindrical ones α is between 12% and 17%. In other words the surface charge density of the spherical micelles is about three times greater than that of the cylindrical micelles. On the other hand, α_s and α_c turn out to be practically independent of ξ (Fig. 11).

The fact that the spherical micelles have ca. three times greater surface charge density than the cylindrical ones (Fig. 11) is important for the understanding of the physical cause of the micelle growth. The fact that $\alpha_s > \alpha_c$ leads to a greater electrostatic energy per monomer incorporated in the spherical micelles: $g_s^{el} > g_c^{el}$. The difference $g_s^{el} - g_c^{el}$ is plotted versus $q \equiv (K_{dl}(X\text{-}X_1))^{1/2}$ in Fig. 12. One sees that $g_s^{el} - g_c^{el}$ increases with the increase of the surfactant concentration, $X-X_1$, and with the decrease of ξ. The mean aggregation number of the micelles, $\bar{n}_M$, behaves in the same way, see Fig. 4 and 7. In other words, the formation of larger cylindrical micelles is energetically more favorable because they bear a lower surface charge, and consequently, they have smaller electric energy (per monomer) than the spherical micelles. In our case $g_s^{el} - g_c^{el}$ is less than $0.06kT$ (Fig. 12), whereas g_s^{el} and g_c^{el}, separately, are about 10 times larger (from 0.67 to $0.76kT$).

In spite of the fact that the difference $g_s^{el} - g_c^{el}$ is relatively small (as compared with g_s^{el} or g_c^{el}) it affects strongly K_{dl} because it enters Eq. (20) multiplied by the aggregation number $n_0 \approx 56$. Fig. 13 shows the calculated growth parameter $K = K_{dl}K_{ndl}$, versus $(X\text{-}X_1)^{1/2}$. Note that the variation of K is in fact due to the variation of K_{dl}, because, as mentioned earlier, the non-double-layer contribution is independent on the surfactant and electrolyte concentration and is determined to be $K_{ndl} \equiv 5.0 \times 10^8$.

It should be noted that in Ref. [6] negative values of the difference $g_s^{el} - g_c^{el}$ are obtained for

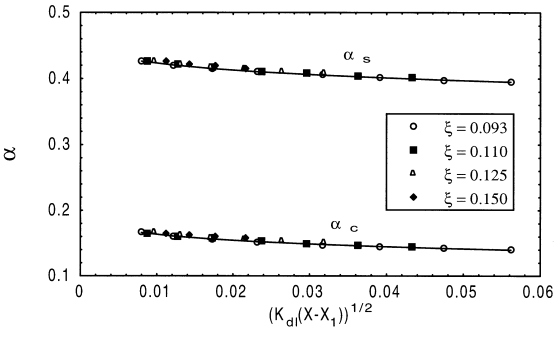

Fig. 11. Degree of surface charging, see Eq. (36), for cylindrical and spherical micelles: α_c and α_s, respectively, plotted versus $[K_{dl}(X-X_1)]^{1/2}$.

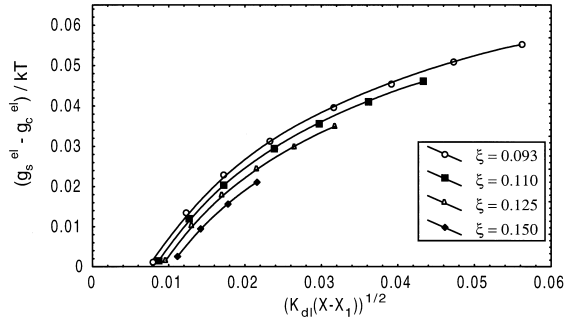

Fig. 12. Difference between the electrostatic energies of a surfactant monomer incorporated in a spherical and cylindrical micelle: g_s^{el} and g_c^{el}, respectively, plotted versus $(K_{dl}(X\text{-}X_1))^{1/2}$ for various ξ.

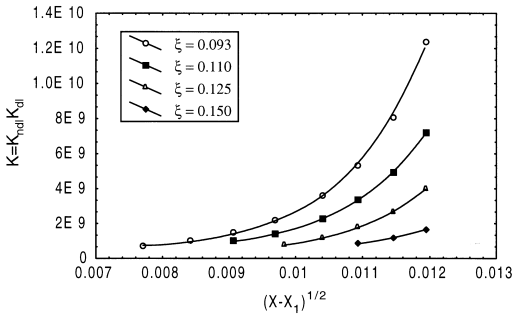

Fig. 13. Calculated growth parameter, K, plotted versus $(X\text{-}X_1)^{1/2}$ for various ξ; the symbols correspond to the experimental points in Fig. 4; see the Appendix A for the procedure of calculations.

the case of 1:1 electrolyte. In contrast, our values of $g_s^{el} - g_c^{el}$ are positive, see Fig. 12. We believe this difference in the sign originates from the different theoretical models used in the two studies. Indeed, Stern layer is not considered in Ref. [6], which is equivalent to assume $\alpha_c = \alpha_s = 1$. On the other hand, we obtain $\alpha_c \approx 0.15$ and $\alpha_s \approx = 0.40$ (see Fig. 11), which affects the difference between the electric energies of the cylindrical and spherical micelles.

Having determined the parameters of the theoretical model, we may then apply it to predict the values of the mass average aggregation number of the micelles, $\bar{n}_M$, for various surfactant and calcium concentrations. Fig. 14(a) and (b) show theoretical curves for $\bar{n}_M$ plotted versus the surfactant (SDP2S) concentration, c_s, for several fixed values of the input calcium concentration, c_{CT}, and for fixed $\delta \equiv 0.55$ nm and ionic strength $I_0 \equiv 128$ mM. The increase of the surfactant concentration, c_s, at *fixed* calcium concentration, c_{CT}, gives rise to two tendencies, acting in the opposite directions: (1) the increase of the surfactant concentration tends to increase the size of the micellar aggregates; (2) on the other hand the increase of c_s at fixed c_{CT} leads to increase of ξ (see Eq. (4), and then to *decrease* of the micelle size, cf. Fig. 4. We should recall that if there were no Ca^{2+} in the solution, only small spherical micelles would form in the concentration range $2 < c_s < 9$ mM (Fig. 14). For the smaller calcium concentrations (Fig. 14(a)), tendency (2) is strong enough to cause a slight decrease of $\bar{n}_M$ with the increase of the surfactant concentration for $c_{CT} = 5$ mM.; for $c_{CT} = 11$ mM

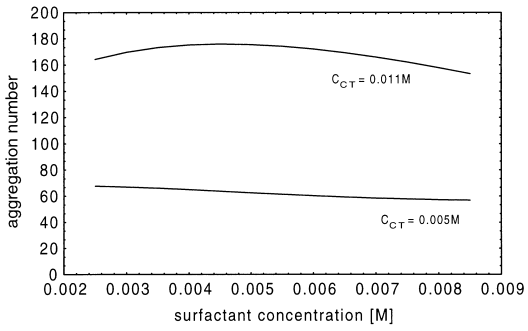

(a)

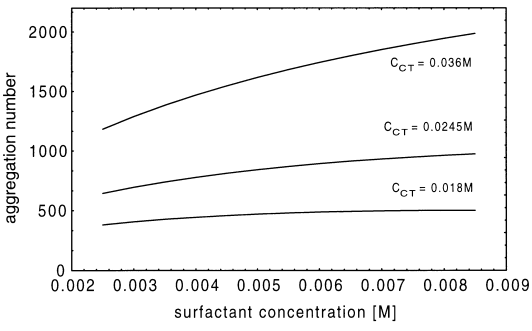

(b)

Fig. 14. Theoretical curves for the mass average aggregation number, $\bar{n}_M$, plotted versus the surfactant (SDP2S) concentration, c_s, for $\delta \equiv 0.55$ nm and several fixed values of the input calcium concentration, c_{CT}: (a) $c_{CT} = 0.005$ and 0.011 M; (b) $c_{CT} = 0.018$, 0.0245 and 0.036 M.

the two tendencies almost counterbalance each other and the plot of $\bar{n}_M$ versus c_s exhibits a maximum. For the higher calcium concentrations (Fig. 14b) $\bar{n}_M$ increases with c_s, as the physical insight would suggest. Fig. 14(a) and (b) allow one to estimate what is the expected average micelle size at given surfactant and calcium concentration.

6. Conclusions

We establish that the "ladder" model [6] is applicable to the micellar solutions of SDP2S in the presence of 1:1 electrolyte, see Fig. 3. However, this is not the case with the solutions of the same surfactant in the presence of $CaCl_2$, see Fig. 4. To solve the problem we undertook additional experi-

mental and theoretical investigations for solutions containing bivalent counterions.

To check whether the light scattering data about the micelle aggregation number is not affected by the micelle–micelle interactions, we carried out independent dynamic and static light scattering measurements of micelle size. The results (see Fig. 2 and the related text) show, that the effect of micelle–micelle interactions is negligible for the investigated solutions.

It turns out that the discrepancy between the ladder model [6] and the experimental data (for solutions with Ca^{2+}) can be removed taking into account the effect of the added electrolyte on the growth parameter, K. We carried out ultrafiltration experiments which revealed that a considerable part (from 24% up to 60%) of the Ca^{2+} ions are associated with the micelles (Fig. 5). We derived an expression, Eq. (13), which allows to estimate the concentration, c_{CB}, of Ca^{2+} remaining in the background solution at a given surfactant concentration, c_s, see Fig. 5(b).

The dependence of c_{CB} on c_s is crucial for the interpretation of the experimental data. Indeed, the growth parameter K depends on c_{CB}, and in addition, c_{CB} increases with the rise of c_s at fixed ξ, see Fig. 5b. This leads to an indirect dependence of K on c_s. In Section 4 we derive the theoretical dependence of K versus c_s; see also Fig. 13. The comparison of theory with experiment shows a good agreement. In particular, the data from all curves in Fig. 4 can be fitted with a single straight line (Fig. 7) as predicted by the ladder model, complemented with the theory from Section 4, see Eq. (41).

The theoretical results from Section 4 allow one to understand what happens in the micelle solution if the surfactant concentration is increased at fixed surfactant-to-Ca^{2+} ratio, ξ. The resulting physical picture is the following. The increase of the surfactant concentration in these experiments is accompanied with an increase of the background Ca^{2+} concentration (Fig. 5(b)). This leads to an increase of the occupancy of the Stern layer of each micelle by adsorbed Ca^{2+} ions (Fig. 9) and to reduction of the surface charge density of the micelles (Fig. 11).

Due to a greater occupancy of the Stern layer by adsorbed counterions the cylindrical micelles have a lower surface charge density and lower electric energy per monomer, g^{el}, compared with the spherical micelles. That is why the formation of cylindrical micelles is energetically more favorable. When rising the surfactant concentration at constant ξ, the difference between the values of g^{el} for spherical and cylindrical micelles increases (Fig. 12), and consequently the fraction of the long rod-like micelles in the solution increases.

Exactly the opposite could happen if the surfactant concentration is increased at constant Ca^{2+} concentration (instead of at constant ξ): the size of the micelles decreases (Fig. 14a, $c_s = 5$ mM), because the relative amount of the Ca^{2+} ions adsorbed on the micelles becomes insufficient to neutralize their surface charges, and then the formation of long rod-like micelles becomes energetically disadvantageous.

An extension of this study to solutions containing Al^{3+} ions has been carried out [17].

Acknowledgment

This work was supported by Colgate-Palmolive Co. and by the Bulgarian National Science Fund. The authors are indebted to Dr K. D. Danov and Mrs Z. Dimitrova for their help in the computer calculations and Ca^{2+} spectro-photometric measurements, respectively.

Appendix A. Procedure of calculations

The aim of the numerical procedure is to fit the experimental data from Fig. 4 plotted as $\bar{n}_M$ versus $q \equiv [K_{dl}(X - X_1)]^{1/2}$ see Eq. (41). $\bar{n}_M$ is determined by the light scattering experiments. In addition, we have $X - X_1 = 0.018(c_s - \mathrm{CMC}) = 0.018 c_{SM}$ where the values of c_s and CMC (in mol/l) are also known from the experiment. Therefore, the main efforts are directed to the calculation of K_{dl} for given values of c_{SM} and ξ.

(1) The input parameters are $R = 2.57 \times 10^{-7}$ cm, $e = 4.8 \times 10^{-10}$ CGSE units, $\epsilon = 77.5$, $\epsilon_{st} = 55.5$, $kT = 4.1 \times 10^{-14}$ erg; the diameters of Na^+ and Ca^{2+} ions are $\delta_N = 0.72$ nm and

$\delta_C = 0.82$ nm, respectively; the aggregation number of the smallest spherical micelles is $n_0 = 56$. The values of ξ for the separate experimental curves are shown in Fig. 4; c_{SM} is an input variable characterizing the experimental points, see also Eq. (18). The constant in the Ca^{2+} adsorption isotherm, Eqs. (12) and (13), is also known: $B = 2.5 \times 10^{-5}$ M.

In the case of *cylindrical* micelle we set

$$m = 1, \quad a = 0.64\ nm^2. \tag{A1}$$

In the case of *spherical* micelle we set

$$m = 2, \quad a = 1.48\ nm^2. \tag{A2}$$

The adjustable parameters are K_{ndl} and the thickness of the Stern layer, δ. From an input value of δ we calculate Φ_C and Φ_N by means of Eqs. (39) and (40).

(2) For given values of c_s and ξ we calculate c_{CT} from Eq. (18), c_{CB} from Eqs. (12) and (13). Then I_t and c_{SM} are calculated from Eqs. (17) and (18), and c_{NB} is calculated from the equation

$$c_{NB} = 2I_t - I_0 - 4c_{CB} + c_{CT} - CMC, \tag{A3}$$

which follows from Eqs. (15) and (16); $I_0 = 0.128$ M and $\alpha_{Na} \approx 0.20$; the results are not sensitive to the value of α_{Na}. Then we calculate κ and λ from Eq. (26).

(3) Further, assuming a tentative value of y_0 we calculate $J(y_0)$, b_N and b_C from Eqs. (33) and (38); $\alpha(y_0)$ is calculated from Eqs. (36) and (37). The results are substituted in the equation

$$\left(\frac{4\pi e^2}{\epsilon kTa\kappa}\right)^2 \alpha^2(y_0) = 4(1-\lambda^2 + \lambda^2 e^{y_0}) \sinh^2\left(\frac{y_0}{2}\right) + \frac{2m}{\kappa R} J(y_0), \tag{A4}$$

stemming from Eqs. (27), (32) and (35); Eq. (A4) is solved numerically to determine y_0. In this way one obtains also the values of θ_C, θ_N and α.

(4) Next we calculate g^{el} by means of Eq. (34) where S and σ are given by Eqs. (32) and (35). The integral in Eq. (34) is to be solved by numerical integration.

(5) The values of g^{el} calculated for cylinder and sphere by using the parameter values given by Eqs. (A1) and (A2) are substituted in Eq. (20) and thus K_{dl} is obtained.

(6) For each experimental value of $X - X_1$ we calculate the quantity $q \equiv [K_{dl}(X - X_1)]^{1/2}$. theoretical value of $\bar{n}_M$ is calculated by means of Eq. (41).

(7) The adjustable parameters δ and K_{ndl} are determined from the fit of the experimental data for $\bar{n}_M$ versus q by means of the least squares method by minimization of the function $\Psi(\delta, K_{ndl})$ in Eq. (42). For $\xi = 0.093$ we obtain $K_{ndl} = (5.00 \pm 0.25) \times 10^8$. Since it is not expected K_{ndl} to depend on ξ we fixed $K_{ndl} = 5.00 \times 10^8$ and processed the data for the other values of ξ($\xi = 0.11$, 0.125 and 0.15, see Fig. 4) with a single adjustable parameter, δ. The best fits gave practically the same values of, $\delta \approx 0.55$ nm, for all ξ (see Table 1), which could be interpreted as an argument in favor of the physical adequacy of the theoretical model.

Finally, let us describe how the values of a_s and a_c in Eqs. (A1) and (A2) are obtained. The procedure is the following:

(a) From the light scattering data we know that $n_0 \approx 56$; in addition, both the light scattering and the calculations based on molecular structure yield $R = 2.57$ nm for the micelle outer radius, at which the centers of the SO_4^- groups are located. Then one obtains the area per SO_4^- group at the surface of a *spherical* micelle to be

$$a_s = \frac{4\pi R^2}{n_0} = 1.48\ nm^2, \tag{A5}$$

(b) Next, we calculate the area per surfactant molecule at the sphere dividing the hydrophobic core of a spherical micelle from its hydrophilic

headgroup region:

$$a_s^{(core)} = \frac{4\pi R_{core}^2}{n_0} = 0.63\ nm^2, \quad (A6)$$

where $R_{core} = 1.67$ nm is the radius of the micelle hydrophobic core; $R_{core} = 1.67$ nm is also the length of a dodecyl chain.

(c) Then we use the "packing constraint" of Israelachvili et al. [16] to calculate the area per surfactant molecule at the dividing surface between the hydrophobic core and the hydrophilic headgroup region of a *cylindrical* micelle:

$$a_c^{(core)} \approx a_s^{(core)}/1.5 = 0.42\ nm^2, \quad (A7)$$

(d) Finally, we estimate the area per SO_4^- group at the surface of a *cylindrical* micelle using the following geometrical relationship:

$$a_c = a_c^{(core)} \frac{R}{R_{core}} = 0.64\ nm^2. \quad (A8)$$

Note that $a_s/a_c = 2.3$, but nevertheless the packing constraint, Eq. (A7), is satisfied.

References

[1] J.N. Israelachvili, Intermolecular and Surface Forces, Academic Press, London, 1991.
[2] R. Tausk, J.Th.G. Overbeek, Colloid Interface Sci. 2 (1976) 379.
[3] D.F. Nicoli, D.R. Dawson, J.W. Offen, Chem. Phys. Lett. 66 (1979) 291.
[4] P.J. Missel, N.A. Mazer, G.B. Benedek, M.C. Carey, J. Phys. Chem. 87 (1983) 1964.
[5] N.A. Mazer, G.B. Benedek, M.C. Carey, J. Phys. Chem. 80 (1976) 1075.
[6] P.J. Missel, N.A. Mazer, G.B. Benedek, C.Y. Young, M.C. Carey, J. Phys. Chem. 84 (1980) 1044.
[7] N.A. Mazer, in: R. Pecora (Ed.), Dynamic Light Scattering, Plenum, London, 1985, ch. 8.
[8] G. Porte, J. Appell, Y. Poggi, J. Phys. Chem. 84 (1980) 3105.
[9] G. Porte, J. Appell, J. Phys. Chem. 85 (1981) 2511.
[10] H. Hoffmann, J. Klaus, H. Thurn, K. Ibel, Ber. Bunsenges. Phys. Chem. 87 (1983) 1120.
[11] J.-M. Chen, T.M. Su, C.Y. Mou, J. Phys. Chem. 90 (1986) 2418.
[12] P.J. Missel, N.A. Mazer, M.C. Carey, G.B. Benedek, J. Phys. Chem. 93 (1989) 8354.
[13] T.-L. Lin, M.-Y. Tseng, S.-H. Chen, M.F. Roberts, J. Phys. Chem. 94 (1990) 7239.
[14] T. Odijk, J. Phys. Chem. 93 (1989) 3888.
[15] R.G. Alargova, J.T. Petkov, D.N. Petsev, I.B. Ivanov, G. Broze, A. Mehreteab, Langmuir 11 (1995) 1530.
[16] J.N. Israelachvili, D.J. Mitchell, B.W. Ninham, J. Chem. Soc., Faraday Trans. 2 (72) (1976) 1525.
[17] R.G. Alargova, K.D. Danov, P.A. Kralchevsky, G. Broze, A. Mehreteab, Langmuir, in press.
[18] H.G. Thomas, A. Lomakin, D. Blankschtein, G.B. Benedek, Langmuir 13 (1997) 209.
[19] T. Kato, M. Kanada, T. Seimiya, J. Colloid Interface Sci. 181 (1996) 149.
[20] P. Mukerjee, J. Phys. Chem. 76 (1972) 565.
[21] D.J. Mitchell, B.W. Ninham, J. Phys. Chem. 87 (1983) 2996.
[22] F.C. MacKintosh, S.A. Safran, P.A. Pincus, Europhys. Lett. 12 (1990) 697.
[23] A. Ben-Shaul, W.M. Gelbart, J. Phys. Chem. 86 (1982) 316.
[24] T. Odijk, J. Chem. Phys. 93 (1990) 5172.
[25] E. Mileva, J. Colloid Interface Sci. 178 (1996) 10.
[26] C. Tanford, The Hydrophobic Effect: Formation of Micelles and Biological Membranes, Wiley, New York, 1980, ch. 7.
[27] M.U. Oko, R.L. Venable, J. Colloid Interface Sci. 35 (1971) 53.
[28] R.G. Alargova, K.D. Danov, J.T. Petkov, P.A. Kralchevsky, G. Broze, A. Mehreteab, Langmuir 13 (1998) 5544.
[29] R.J. Hunter, Foundations of Colloid Science, Clarendon Press, Oxford, 1987.
[30] E.Y. Sheu, S.-H. Chen, J. Phys. Chem. 92 (1988) 4466.
[31] J.F. Scamehorn, S.D. Christian, R.T. Ellington, in: J.F. Scamehom, T.H. Harwell (Eds.), Surfactant Based Separation Processes, Marcel Dekker, New York, 1989.
[32] A. Hafiane, I. Issid, D. Lemorandt, J. Colloid Interface Sci. 142 (1991) 167.
[33] D.J. Miller, Colloid Polym. Sci. 267 (1989) 929.
[34] E.J.W. Verwey, J.Th.G. Overbeek, Theory of the Stability of Lyophobic Colloids, Elsevier, Amsterdam, 1948.
[35] P.H. Wiersmaa, A.H. Loeb, J.Th.G. Overbeek, J. Colloid Interface Sci. 22 (1966) 78.
[36] W.C. Chew, P.N. Sen, J. Chem. Phys. 77 (1982) 2042.
[37] B.V. Derjaguin. Theory of Stability of Colloids and Thin Films, Plenum Press, New York, 1989.
[38] E.D. Shchukin, A.V. Pertsov, E.A. Amelina, Colloid Chemistry, University Press, Moscow, 1982 (in Russian).
[39] A.W. Adamson, Physical Chemistry of Surfaces, Wiley, New York, 1976.